The October 28, 2012 M_w 7.8 Haida Gwaii underthrusting earthquake and tsunami: Slip partitioning along the Queen Charlotte Fault transpressional plate boundary

Thorne Lay [a], Lingling Ye [a], Hiroo Kanamori [b], Yoshiki Yamazaki [c], Kwok Fai Cheung [c], Kevin Kwong [d], Keith D. Koper [d]

[a] *Department of Earth and Planetary Sciences, University of California Santa Cruz, Santa Cruz, CA 95064, USA*
[b] *Seismological Laboratory, California Institute of Technology, Pasadena, CA 91125, USA*
[c] *Department of Ocean and Resources Engineering, University of Hawai'i, Honolulu, HI 96822, USA*
[d] *Department of Geology and Geophysics, University of Utah, Salt Lake City, UT 84112, USA*

Supplementary Information Figures S1-S8, Animations S1-S3

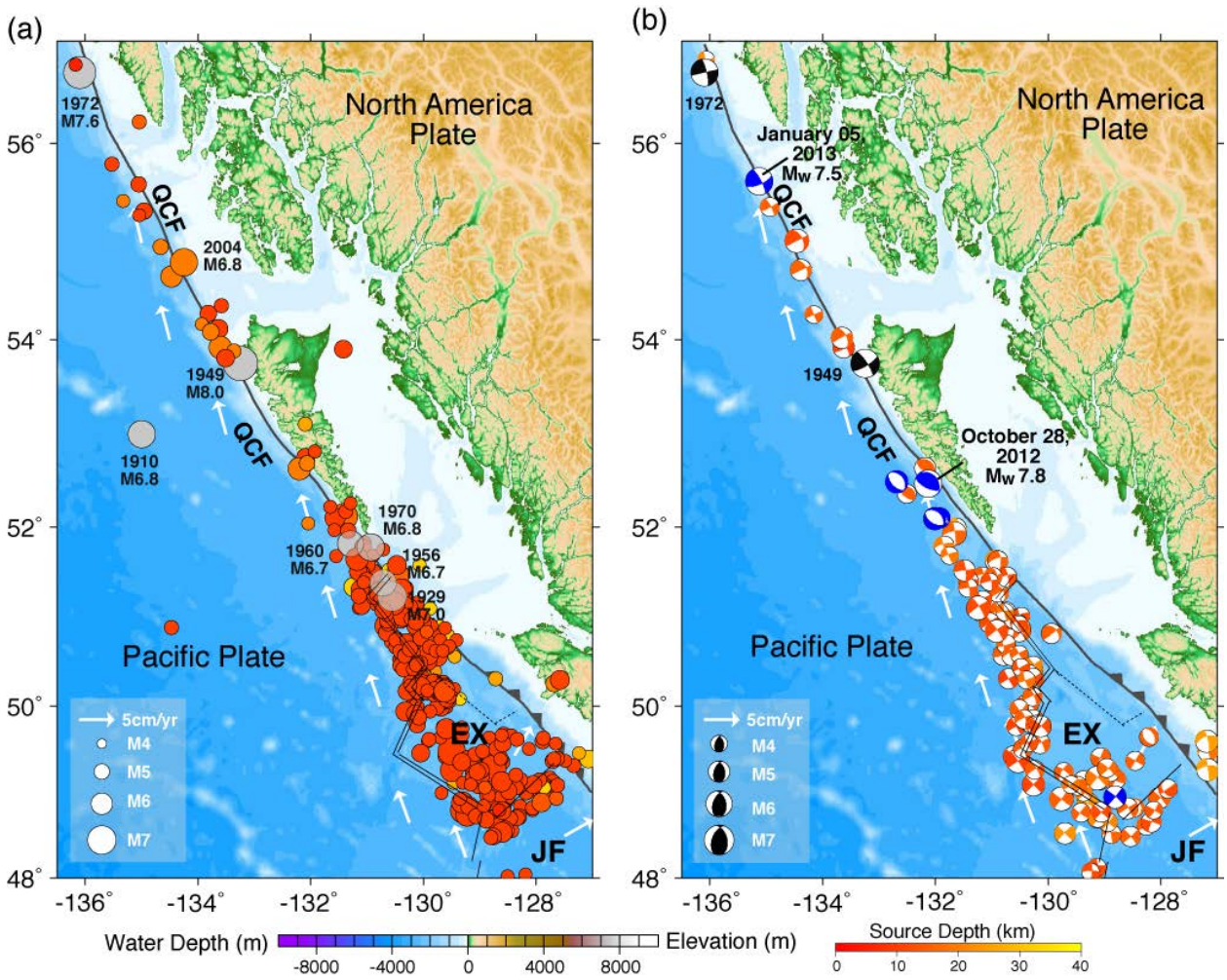

Fig. S1. Regional historical seismicity maps: (a) USGS/NEIC catalog earthquake locations for $m_b \geq 4.5$ (circle size is proportional to magnitude and color indicates source depth) from 1973 up to just before the October 28, 2012 event, along with $M \geq 6.5$ events (gray circles) from 1900 to 1973 from PAGER-CAT (Allen et al., 2009); and (b) the best double-couple of moment tensor solutions from the Global CMT catalog from 1976-2012, plotted at the centroid locations. Arrows indicate Pacific plate and Juan de Fuca plate motion direction and rate relative to the North America Plate computed using model NUVEL-1 (Argus and Gordon, 1991).

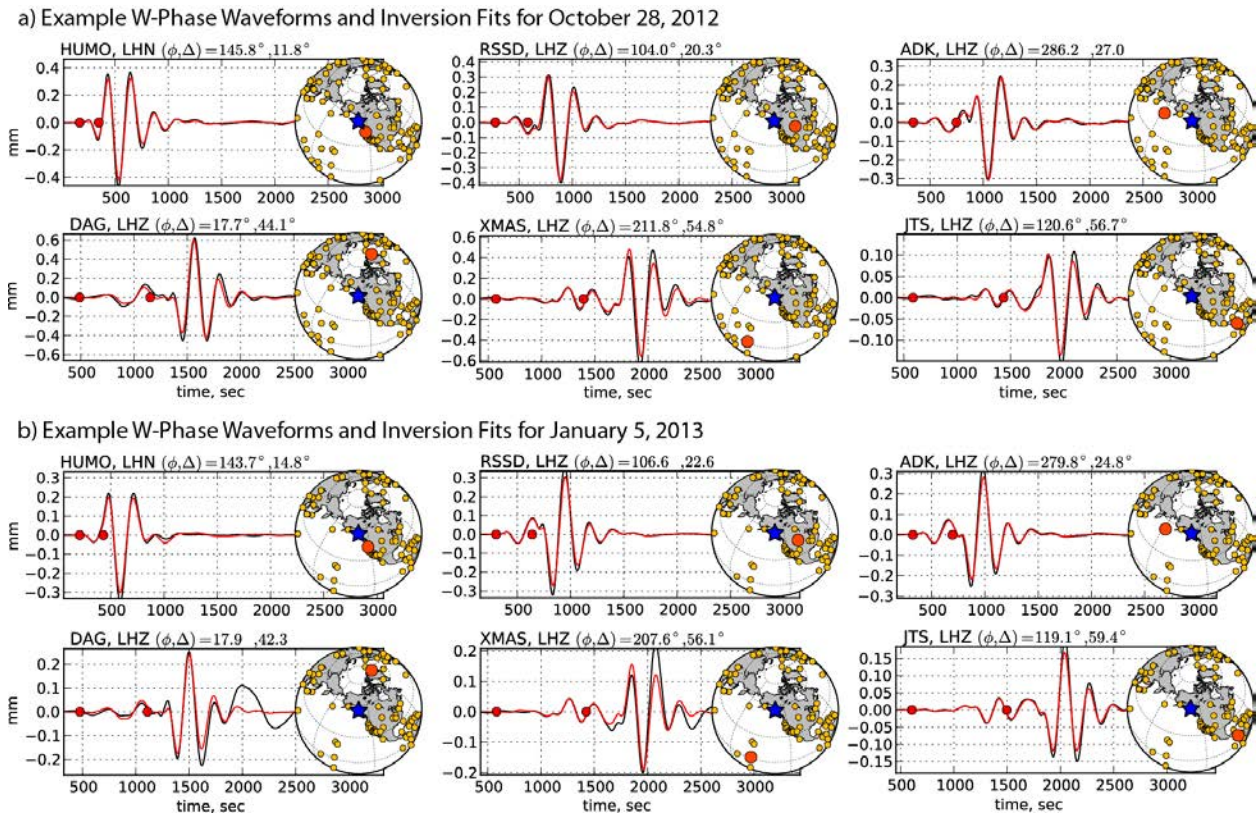

Fig. S2. Example W-phase observations (black traces) and computed waveforms (red) for the point-source moment tensors in Figure 2 for a) October 28, 2012 Haida Gwaii and b) January 5, 2013 Queen Charlotte Fault events. The data are from global seismic network stations with ground displacement filtered in the frequency band 0.00167-0.005 Hz. The W-phase signal used in the inversions is the waveform interval between the red dots. The large amplitude signals after the W-phase are fundamental mode surface waves and the waveform comparisons are predictions for those signals. The maps indicate the position of the station (red dot) among the total set of stations (gold dots) used in the corresponding W-phase inversion. Station DAG for the 2013 event has some non-linear response following the surface wave, well outside the W-phase window. Comparable waveform matches are found for all of the stations indicated in the maps.

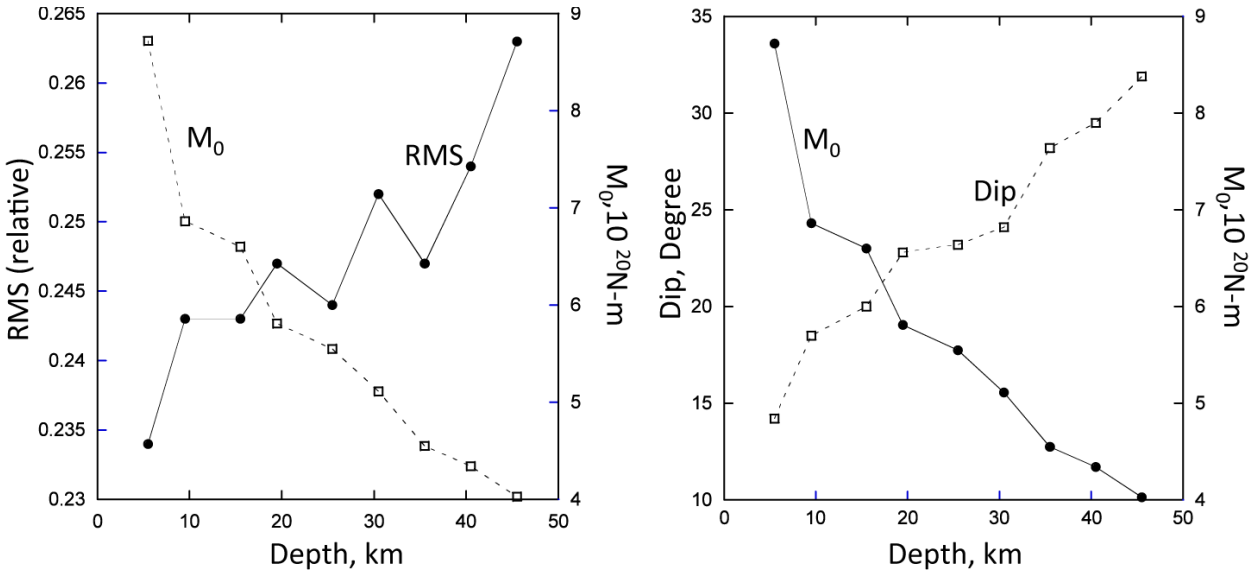

Fig. S3. Results of W-phase inversions for different source depths for the October 28, 2012 Haida Gwaii event. On the left, the relative waveform RMS residual is shown as a function of centroid depth, along with the seismic moment (M_0) estimate for each source depth. On the right the dip for the best-double couple mechanism for each moment tensor is shown for various centroid depths. As the dip decreases the seismic moment increases.

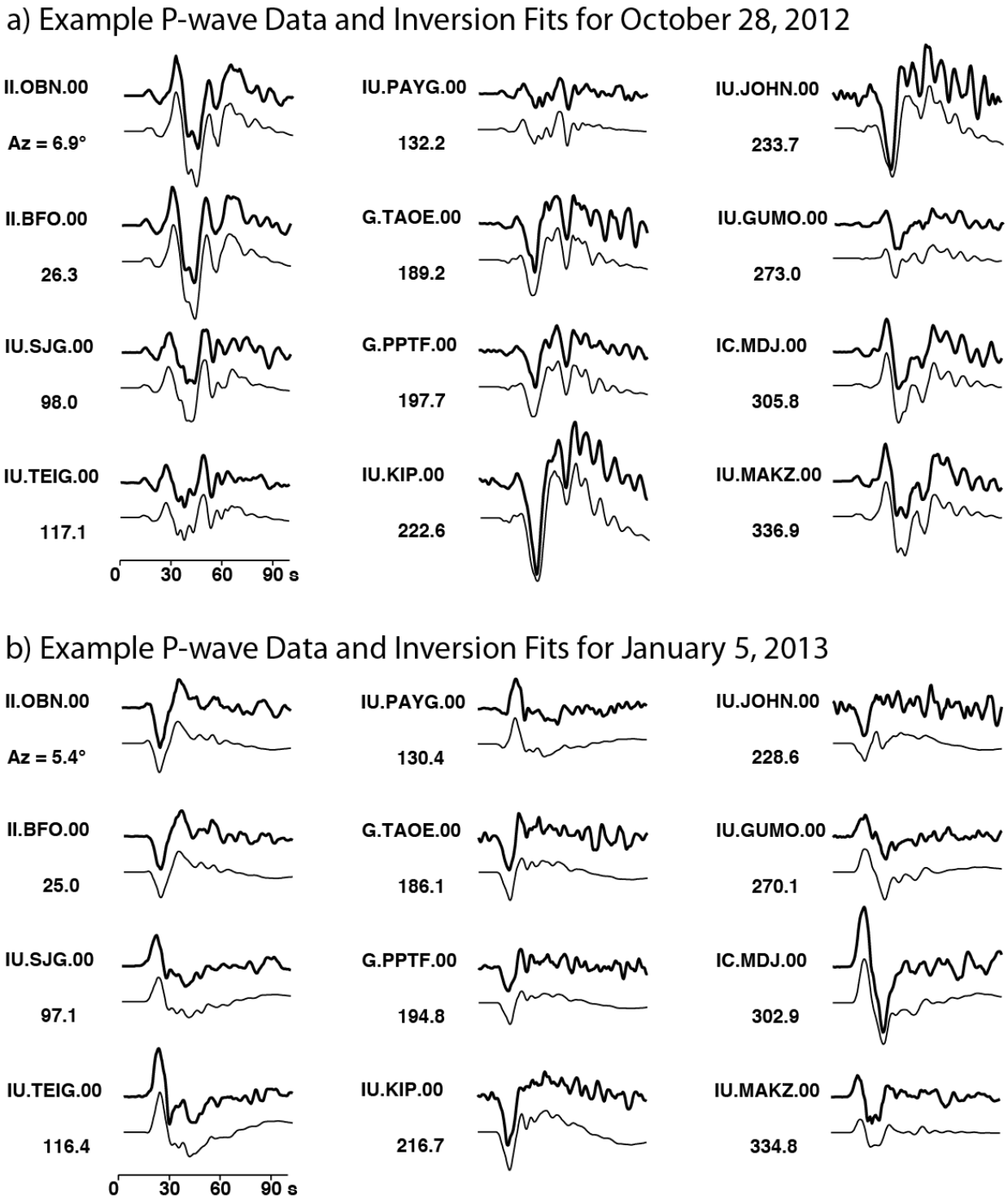

Fig. S4. Comparison of observed (bold lines) and modeled (thin lines) broadband P waves for the **a)** October 28, 2012 Haida Gwaii and **b)** January 5, 2013 Queen Charlotte Fault earthquakes. In both cases the models shown in Figure 3 are used for the computations. The signals are broadband ground displacements in the passband 0.005-0.9 Hz. Comparable waveform matches are found for all of the stations used in the inversions.

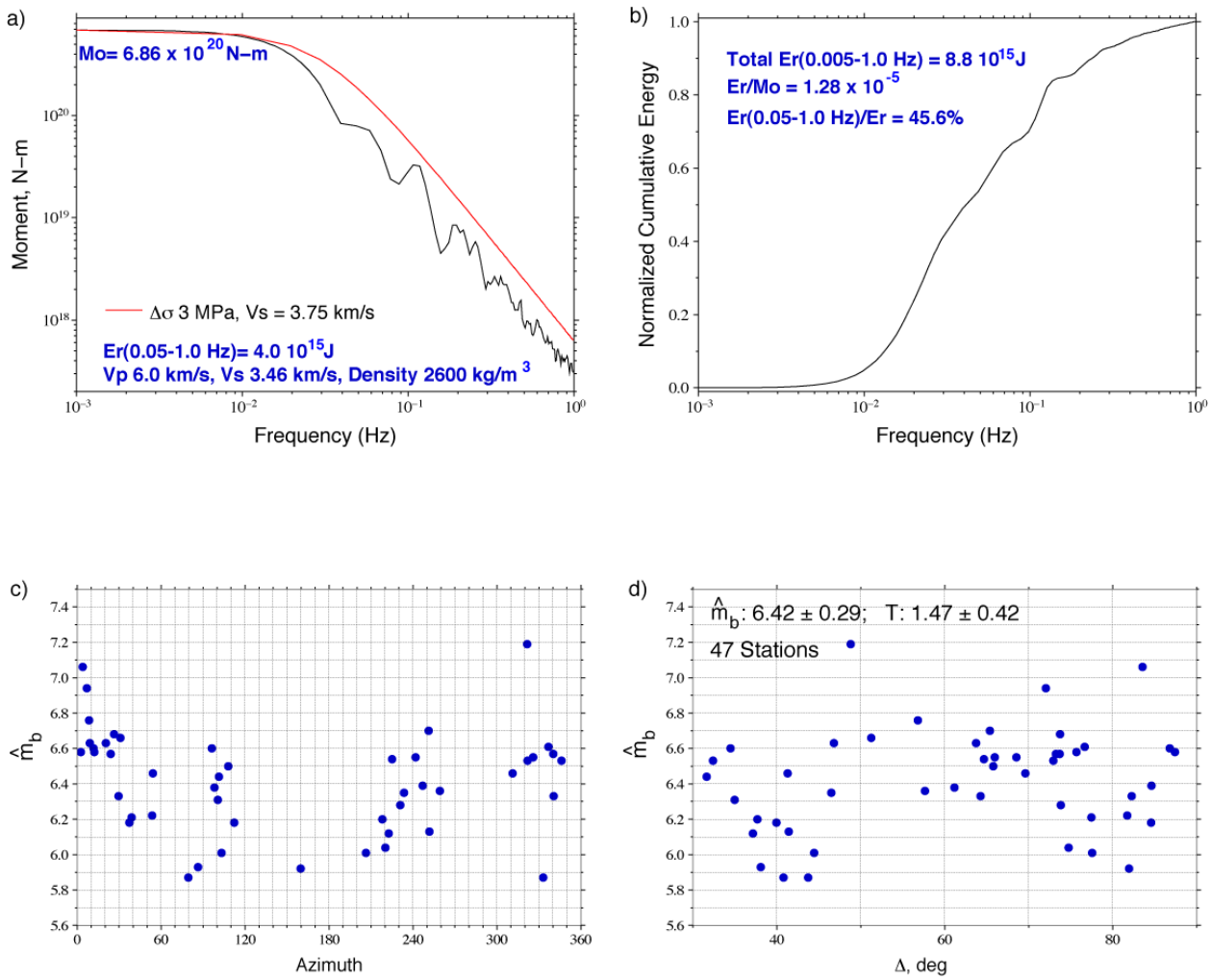

Fig. S5. a) Source spectrum for the October 28, 2012 Haida Gwaii M_w 7.8 event earthquake obtained from combining the spectrum of the finite-source model from P wave inversion (Figure 3) for frequencies below 0.05 Hz with a averaged spectra of broadband P waves for frequencies from 0.05 to 1.0 Hz. The radiated energy from the latter passband is 4.0 x 10^{15} J. A reference ω-squared source spectrum with a stress drop parameter of 3 MPa is shown for comparison. b) Cumulative energy as a function of frequency over the passband from 0.005 to 1.0 Hz, with a total energy, Er, of 8.8 x 10^{15} J. The ratio of Er/M_0 = 1.28 x 10^{-5}. c) Azimuthal pattern of short-period $\hat{m}_b$ measurements. d) Distance distribution of short-period $\hat{m}_b$ measurements, along with the average value of 6.42 for 47 stations.

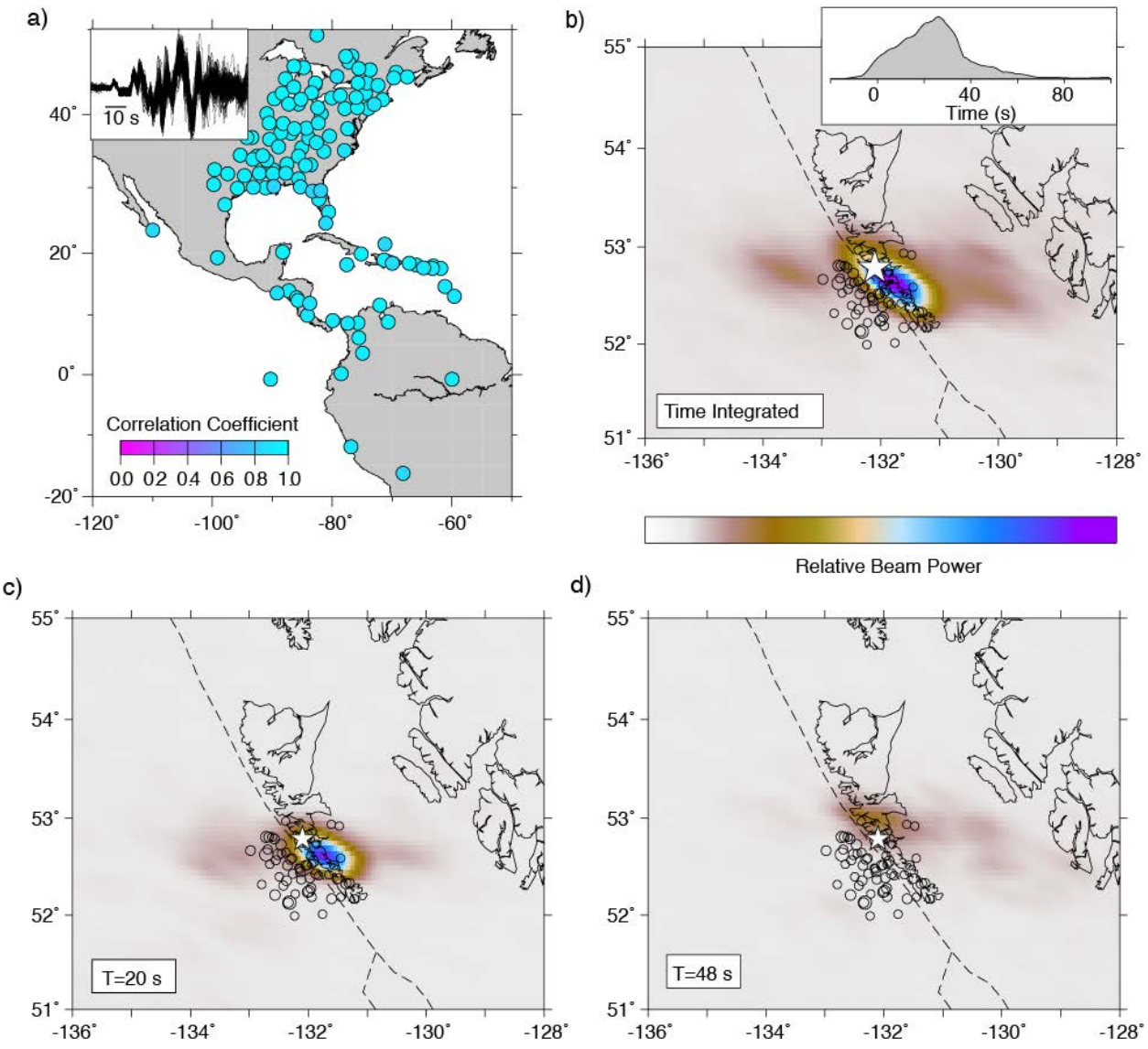

Fig. S6. a) Map of station locations toward the southeast from the 2012 Haida Gwaii earthquake with superimposed broadband waveforms and correlation coefficients for each station being indicated by the color scale. **b)** Map of the relative power of time-integrated coherent short-period (0.5-2.0 s) P wave radiation from the October 28, 2012 Haida Gwaii event imaged by back-projection of the signals from the 117 stations in **a)**, with power ranging from zero (white) to unity (purple). **c)** Snapshot at 20 s into the rupture indicating the back-projected beam power showing radiation from SE of the hypocenter. **d)** Snapshot at 48 s into the rupture indicating the back-projected beam power showing radiation from NW of the hypocenter. Animations of the full time sequence is shown in Animation S1.

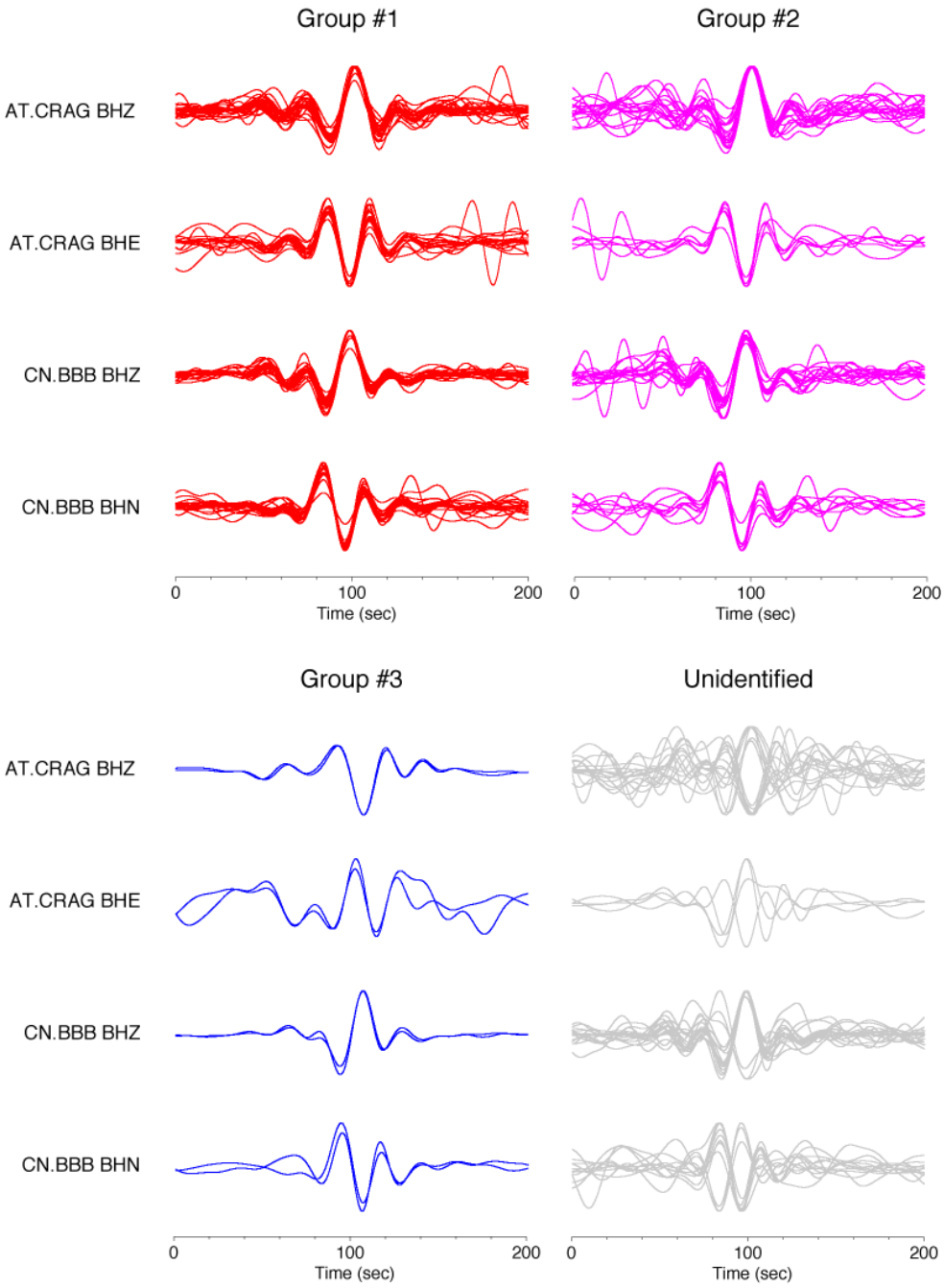

Fig. S7. Superposition of amplitude-scaled waveforms for 20-100 s period signals from aftershocks of the October 28, 2012 Haida Gwaii earthquake sorted into 4 groups. Groups #1 and #2 are probably all normal faulting events given the high correlation with waveforms for Reference event 1, which has a GCMT normal faulting solution. High correlations of vertical and horizontal components at stations CRAG and BBB are found for these groups with all positive correlation coefficients in the range 0.6-1.0 for assignment to Group #1 and positive correlations greater than 0.5 for assignment to Group #2. Group #3 involves oblique slip events with distinct waveforms. Unidentified events have waveforms that may have high noise or mixed sign correlations between stations and components. Most may be normal faulting, but a few are clearly distinct.

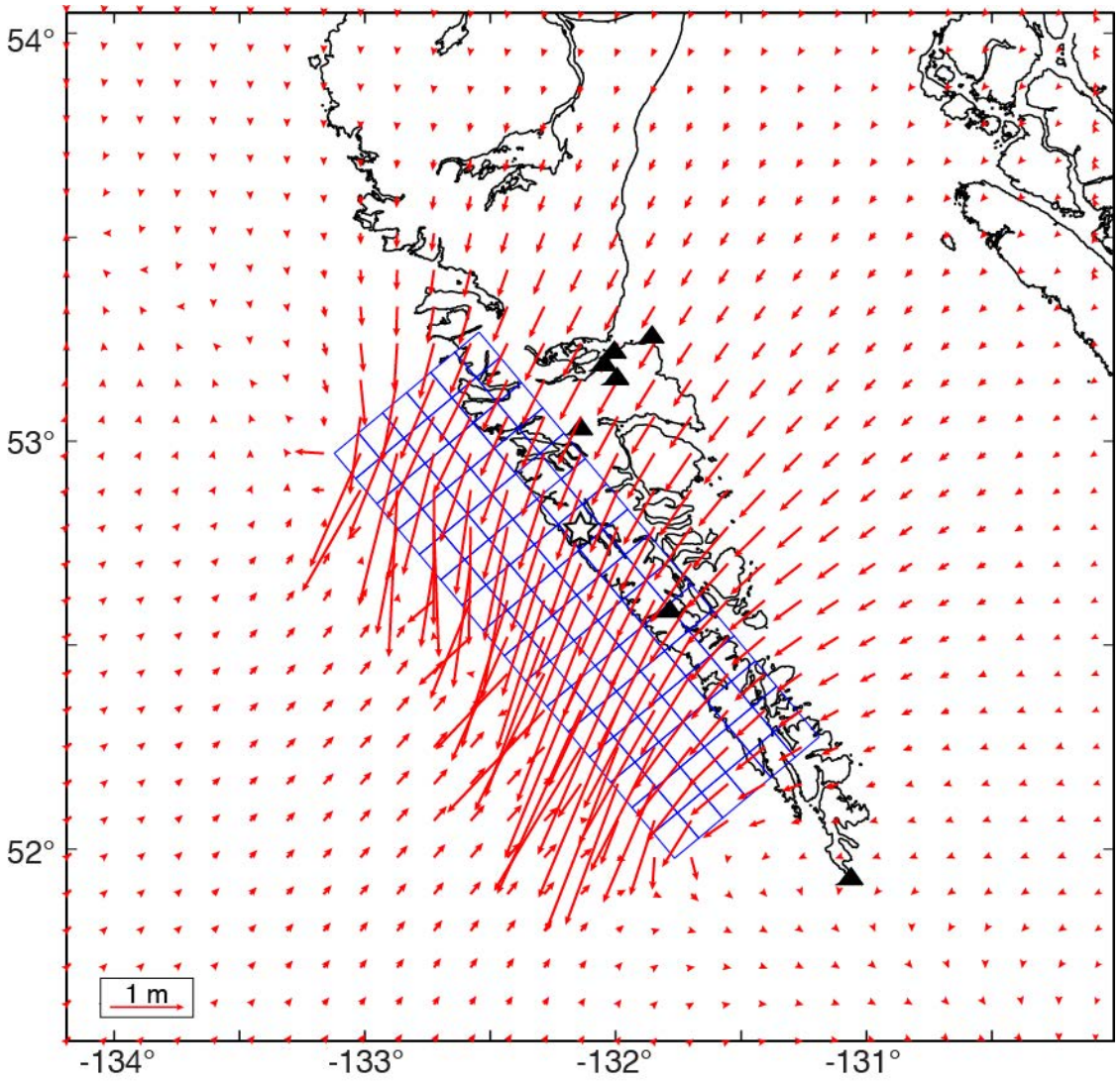

Fig. S8. Horizontal surface displacements predicted for the preferred fault model for the October 28, 2012 Haida Gwaii earthquake. The star indicates the USGS epicentral location on the surface projection of the 18.5° dipping model grid (rectangle). The triangles indicate locations of campaign and high-rate GPS stations. Data from those stations are not yet distributed.

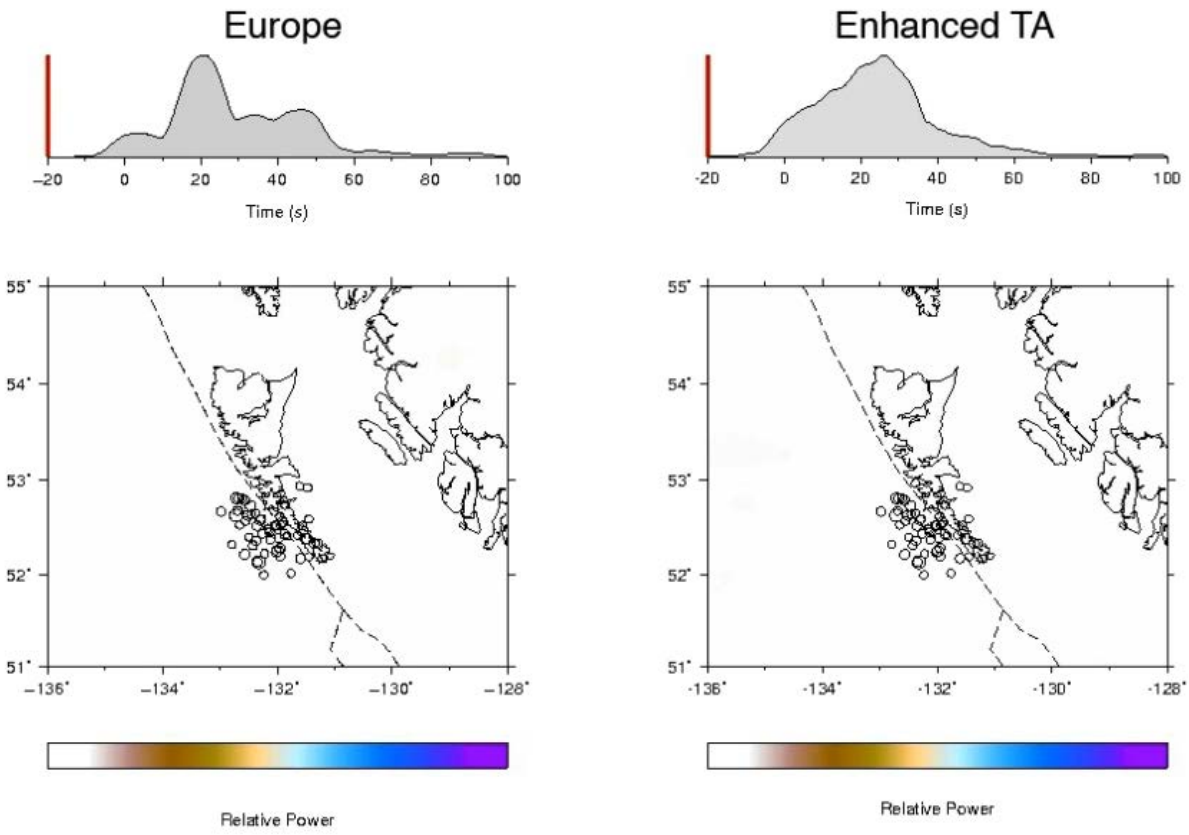

Animation S1. Time-sequence animations of the back-projections of the teleseismic short-period P waves recorded in Europe (Figure 4) and at azimuths to the southeast (Figure S4) for the October 28, 2012 Haida Gwaii earthquake. The relative power of the beam at each position around the source region, normalized the peak beam power for the entire time sequence is shown by the color scale, ranging from zero (white) to unity (purple).

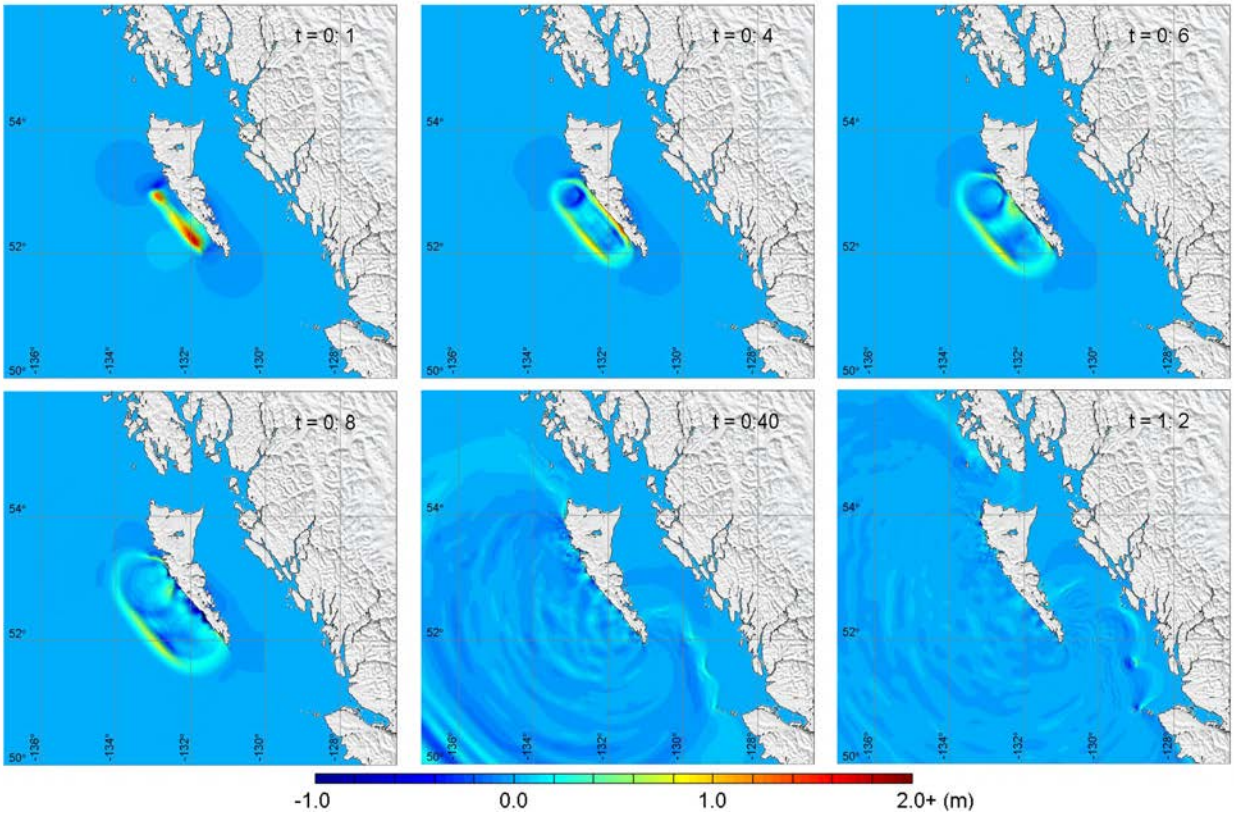

Animation S2. Time evolution of the computed sea surface showing tsunami generation and propagation near the rupture area.

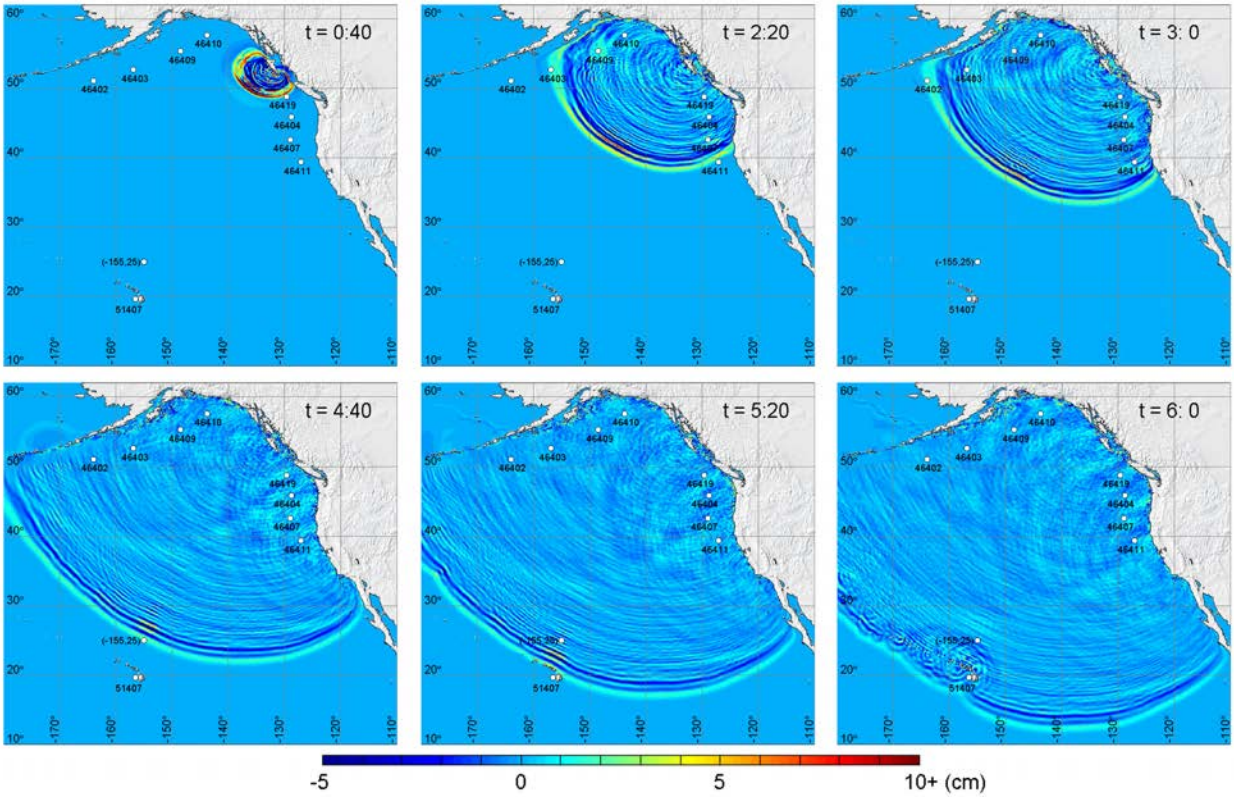

Animation S3. Time evolution of the computed sea surface showing tsunami propagation over northeast Pacific. White circles indicate water level stations.

Table S1. Aftershock event categories (1-normal fault, 2-likely normal fault, 3-oblique, 4 unidentified)

	Date	Time	Lon.	Lat.	Category
001	10/28	030408.82	-132.1	52.79	Main
002	10/28	091727.70	-132.01	52.24	1
003	10/28	093635.00	-132.37	52.36	2
004	10/28	102308.58	-132.67	52.81	1
005	10/28	102415.63	-131.83	52.3	2
006	10/28	104548.00	-132.52	52.48	2
007	10/28	105031.00	-132.23	52.48	4
008	10/28	112745.67	-132.13	52.45	1
009	10/28	115318.00	-132.37	52.36	4
010	10/28	120940.86	-132.45	52.64	4
011	10/28	130914.33	-131.87	52.43	1
012	10/28	150655.08	-132.16	52.42	2
013	10/28	154458.92	-132.42	52.31	1
014	10/28	154845.80	-132.26	52.43	2
015	10/28	155716.00	-132.69	52.68	4
016	10/28	155911.46	-132.57	52.79	1
017	10/28	161703.37	-131.56	52.52	4
018	10/28	185420.83	-132.6	52.67	1
019	10/28	190321.85	-132.67	52.83	1
020	10/28	190953.90	-132.08	52.29	1
021	10/28	191650.76	-132.48	52.65	1
022	10/28	212904.08	-132.12	52.4	1
023	10/28	224127.95	-131.97	52.39	1
024	10/28	231119.28	-132.38	52.65	4
025	10/28	232650.45	-132.46	52.73	1
026	10/28	233423.46	-132.3	52.58	2
027	10/28	235502.03	-131.47	52.92	2
028	10/29	014901.62	-132.04	52.52	1
029	10/29	024052.99	-132.49	52.4	2
030	10/29	024547.94	-132.84	52.23	4
031	10/29	034755.25	-132.16	52.49	2
032	10/29	053251.69	-132.64	52.35	2
033	10/29	060353.25	-132.4	52.94	1
034	10/29	073905.66	-131.79	52.36	4
035	10/29	120514.33	-132.57	52.58	1
036	10/29	150106.89	-131.76	52.01	4
037	10/29	151501.93	-132.27	51.99	4
038	10/29	163308.32	-131.9	52.26	2

	Date	Time	Lon.	Lat.	Category
039	10/29	173602.63	-131.89	52.17	2
040	10/29	195335.01	-131.84	52.45	2
041	10/29	201426.47	-132.68	52.56	2
042	10/29	204946.88	-131.49	52.38	3
043	10/29	220033.09	-132.29	52.59	1
044	10/30	003217.14	-132.23	52.51	4
045	10/30	003509.60	-131.67	52.47	1
046	10/30	024902.27	-131.9	52.37	1
047	10/30	025508.00	-132.12	52.22	2
048	10/30	044015.38	-131.8	52.19	1
049	10/30	141059.00	-132.23	52.3	1
050	10/30	173329.27	-132.69	52.4	4
051	10/30	44838.08	-132.55	52.37	2
052	11/01	31601.50	-132.02	52.55	1
053	11/01	32713.42	-132.19	52.42	1
054	11/02	25455.00	-130.85	51.67	4
055	11/02	71540.52	-131.94	52.19	4
056	11/02	81954.79	-132.34	52.13	1
057	11/02	083710.44	-132.22	52.22	1
058	11/03	042519.80	-132.01	52.52	1
059	11/03	094823.48	-132.65	52.53	4
060	11/03	121842.45	-132.79	52.32	1
061	11/03	174911.74	-132.33	52.38	1
062	11/04	050754.29	-131.67	52.68	2
063	11/04	074216.00	-131.78	52.76	2
064	11/04	085506.14	-131.79	52.45	1
065	11/04	122732.00	-132.56	52.21	1
066	11/04	131711.74	-131.7	52.45	4
067	11/04	182717.15	-132.42	52.53	1
068	11/06	102702.24	-131.3	52.31	3
069	11/07	150423.50	-133.07	52.66	4
070	11/12	65043.51	-131.5	52.22	4
071	11/12	72601.29	-131.56	52.23	4
072	11/13	43127.72	-132.45	52.9	2
073	11/13	44656.86	-132.62	52.85	4
074	11/13	45545.00	-132.03	52.71	4
075	11/13	73419.00	-132.61	52.81	2
076	11/14	30445.01	-130.65	51.83	4